Available online at www.sciencedirect.com
SCIENCE DIRECT
Catalysis Today 107–108 (2005) 40–45
CATALYSIS TODAY
www.elsevier.com/locate/cattod

The electronic structure of vanadium antimonate A theoretical study

Beatriz Irigoyen [a,*], Alfredo Juan [b], Susana Larrondo [a], Norma Amadeo [a]

[a] *Laboratorio de Procesos Catalíticos, Departamento de Ingeniería Química, Facultad de Ingeniería, Universidad de Buenos Aires, Pabellón de Industrias, Ciudad Universitaria, 1428 Buenos Aires, Argentina*
[b] *Depto. Física-UNS, Avda. Alem 1253, 8000 Bahía Blanca, Argentina*

Available online 15 August 2005

Abstract

The electronic structure of $VSbO_4$ exhibits similarities with that of other metal transition oxides with rutile-type structure, showing O 2s, O 2p, Sb and V bands well differentiated. At lower energy (at −34 eV), there is a band formed by O 2s orbitals with some Sb 5s (bottom) and Sb 5p (top). The Sb 5s orbitals appear in the −20 eV energy region, while around −14 eV there are O 2p states (metal–oxygen bonding) and also some Sb 5p orbitals contributions.

At the Fermi level it can be observed the contribution of V 3d orbitals, which is in agreement with the metal character that vanadium gives to VO_2 in the rutile phase. The V 4s and V 4p orbitals can be found higher in energy.

On the other hand, the analyses of the electronic populations of the $VSbO_4$ catalyst doped with titanium show that partial substitution of Sb by Ti provokes V-cations oxidation. This occurs mainly by depopulating V 3d antibonding states located around the Fermi level and results in V–O bonds reinforcement. Those vanadium cations in a higher oxidation state improve the catalyst surface reoxidation step, suggesting that Sb partial substitution by Ti gives a more active catalyst.

The effect of the Ti-doping on the reaction rate limiting step is also discussed.

Keywords: $VSbO_4$; Ti-doped V–Sb oxides; Electronic structure; DOS; COOP

1. Introduction

Vanadium antimonate catalysts are efficient for hydrocarbons (amm)oxidation reactions. Particularly, the well-established area of selective *o*-xylene oxidation to phthalic anhydride working catalysts is based on V oxides supported on TiO_2 but strongly doped with Sb, Nb and Cs [1]. From the composition of the obtained solids by Sb doping, it was surmised that $VSbO_4$ rutile phase formation improves their selectivity.

Birchall and Sleight were the first to report the $VSbO_4$ rutile phase [2]. These authors showed from a Mössbauer analyses that Sb cations are present in this solid as Sb^{5+} ions. It was reported later that vanadium antimonate catalysts exhibit a rutile-type structure with vanadium cations present in the bulk as V^{3+} and V^{4+}. Moreover, this structure presents cation vacancies with different metal–oxygen probable combinations: $OSb_2\,\square$, OSbV □ and $OV_2\,\square$ (□ represents a cationic vacancy) [3].

Effective catalysts for partial oxidation reactions are multifunctional in nature and possess several key properties, including active sites which are composed of two vicinal metal oxide moieties of optimal metal–oxygen bond strengths, both of which are readily reducible and reoxidizable. To achieve desired product selectivity, the individual active sites must be spatially isolated from each other and be either capable of dissociating dioxygen and of incorporating it into the lattice of the solid catalyst [4]. It was reported that active sites of antimony-based selective alkenes oxidation catalysts are composed of bridging oxygen atoms associated with Sb^{3+} (α-H abstraction) and Sb^{5+} (oxygen insertion into

* Corresponding author.
E-mail address: beatriz@di.fcen.uba.ar (B. Irigoyen).

0920-5861/$ – see front matter © 2005 Elsevier B.V. All rights reserved.
doi:10.1016/j.cattod.2005.07.055

the hydrocarbon fragment) cations. However, for such sites to operate effectively additional elements with facile redox couples positioned in the proximity of the catalytic sites are required. The latter are the reoxidation sites, providing a constant source of lattice oxygen to the active site as it becomes reduced through the oxidation cycle [4].

In a recent quantum-mechanics study of toluene interactions on $VSbO_4$(1 1 0), we have reported possible routes to benzaldehyde and carbon oxides formation [5].

From the adsorption energy calculations we found that total oxidation products are the most favorable ones. These products can be formed due to very strong toluene–V interactions with the solid surface V–O–V chains, involving carbon skeleton and carbon oxides production.

On the other hand, benzaldehyde formation has proved to be a favorable alternative. Moreover, a possible mechanism for the aldehyde formation has been suggested. This route begins with an H-abstraction from the methyl group, which involves the Sb cation participation, and the benzyl-type species formation. This Sb participation is in accordance with the reported role of the Sb^{3+}–O sites in α-H abstraction from propylene, along with propane ammoxidation reactions on V–Sb oxide catalysts [4]. In addition, we found that phenyl–V cation antibonding interaction improves the electronic transference from methyl group to oxide and helps to weaken the C–H bond in the methyl group. The proposed mechanism continues with another H-abstraction from the CH_2 fragment in the desorbed benzyl-type species. Finally, oxygen insertion into the organic fragment gives rise to the benzaldehyde desorption [5].

The selective oxidation products obtained leaves an oxygen vacancy in the solid surface. As a consequence a reduced surface site is formed, which is subsequently reoxidized via lattice oxygen (O^{2-}) coming from an adjacent reoxidation site. Then, faster reoxidation of the catalyst active sites is required to ensure its activity. In catalyst based on antimonates, that function was ascribed to V^{4+} cations [4].

On the other hand, it has been reported that partial substitution of antimony by titanium would provoke V^{3+} cations oxidation [6].

Then, in this work we have studied the electronic structure of the rutile-type $VSbO_4$ and Ti-doped $VSbO_4$ phases in order to evaluate titanium-doping influence to enhance the selective behavior of vanadium antimonate catalysts. Our calculations were performed using the extended Hückel method [7–9], an approximate molecular orbital scheme, implemented with the YAeHMOP package [10]. This method is not reliable for energy and geometry optimization, but captures efficiently the essential orbital interactions. Although the obtained results are approximate, this semi empirical code has allowed us to evaluate properly the changes in electronic configurations of toluene and catalyst active sites due to hydrocarbon interactions [11]. Thus, this code becomes particularly attractive to study the electronic structure of very complex catalysts based on transitions metal oxides like vanadium antimonate.

Table 1
Atomic parameters

Atom	Orbital	IP (eV)	ξ_1	ξ_2	c_1	C_2
V	4s	−8.81	1.300			
	4p	−5.52	1.300			
	3d	−11.00	4.750	1.700	0.4755	0.7052
Sb	5s	−18.80	2.323			
	5p	−11.70	1.999			
O	2s	−32.30	2.275			
	2p	−14.80	2.275			

The atomic parameters used in this work: ionization potential (IP), Slater exponents (ξ_i) and linear coefficients (c_i) are those reported by Hoffmann et al. for O, V and Sb atoms [8,12,13]. These parameters are listed in Table 1.

The off-diagonal Hamiltonian matrix elements have been computed with the modified Wolfsberg-Helmholtz formula [14].

A 40 k-point set for average properties calculations was obtained according to the geometrical method of Ramirez and Böhm [15,16].

We have also analyzed the density of states (DOS) and the crystal orbital overlap population (COOP) to understand metal–oxygen interactions better on V–Sb oxides. The DOS curve is a plot of the number of orbitals per unit volume per unit energy. The COOP curve is a plot of the overlap population weighted DOS versus energy. Integration of the COOP curve up to the Fermi level (E_F) gives the total overlap population of the bond specified. Looking at the COOP, we may analyze the extent to which specific states contribute to a bond between atoms or orbitals [9].

2. Results and discussion

First, we have studied the electronic structure of TiO_2, VO_2 and Sb_2O_4 in rutile phase in order to understand better that of V–Sb oxide and vanadium antimonate doped with titanium.

The primitive unit cell for AB_2 compounds with rutile structure is shown in Fig. 1a. In this structure each metal atom A coordinates octahedrically with the six nearest

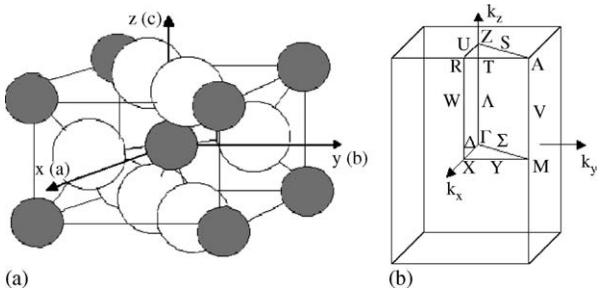

Fig. 1. (a) Primitive unit cell for AB_2 compounds with rutile structure. A: grey, B: empty. (b) Brillouin zone for the tetragonal Bravais lattice with $c/a < 1$.

oxygen atoms B. Each unit cell contains two AB_2 molecules, or a total of six atoms.

The Bravais lattice is tetragonal with $c/a < 1$. The corresponding Brillouin zone is shown in Fig. 1b, where the standard notation is used to identify symmetry points and lines.

3. TiO_2

TiO_2 is a semiconductor with a wide separation between the top of the valence band and the bottom of the conduction band (*band-gap*).

The calculations include only valence orbitals: Ti 3d, 4s, 4p and O 2s, 2p. Thus, the resulting band structure splits into five groups as expected from the simple ligand field arguments. The band at −33 eV is basically formed by O 2s orbitals. Around −16 eV the band corresponding to O 2p orbitals (70–100% O, 0–30% Ti; depending on the band specific energy and the evaluated k point) appears. In the same energy zone, the peaks in the DOS curve show the hybridization of the corresponding molecular orbitals.

The band at −10 eV corresponds basically to Ti 3d (t_{2g}) orbitals; while that above −5 eV is formed basically by Ti 3d (e_g) orbital contributions and some Ti 4s.

The Fermi level falls at the top of the valence band ($E_F = -14{,}447$ eV), while the metal bands Ti 4s and Ti 4p appear higher in energy.

The theoretical results obtained for the electronic structure of TiO_2 show an essential agreement with those reported in Ref. [17]. The band-gap of 3.5 eV between valence band O 2p and conduction band Ti 3d is comparable to the measured values (3.0–3.3 eV) [18].

4. VO_2

This oxide on the studied structure has one electron in the V 3d band and this gives metal conductivity to the high temperature phase.

Fig. 2 shows the band structure and density of states of VO_2. The 3D periodic structure has been obtained from a unit cell composed of two metal atoms and four oxygen atoms. At −33 eV four bands composed by O 2s orbitals can be seen. Above the twelve O 2p bands located around −15 eV are the 10 metal d bands. These bands split in the six-fold-degenerate t_{2g} sub-bands, near −10 eV and the four-fold-degenerate e_g sub-bands, higher in energy around −5 eV. The Fermi level falls at the bottom of the t_{2g} band ($E_F = -10.383$ eV).

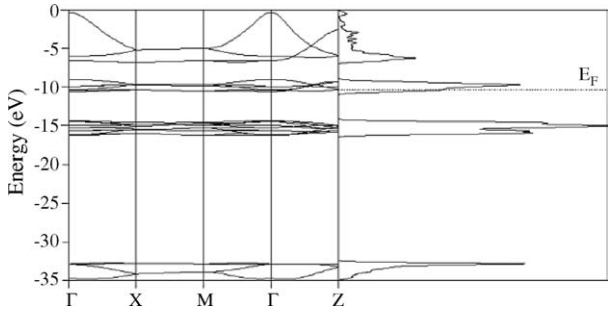

Fig. 2. Band structure along selected symmetry points (left) and total density of states (right) for the crystal 3D structure of VO_2. The doted line indicates the Fermi level (E_F).

On the right of Fig. 2 around −33 eV contributions from O 2s orbitals and some V 4s can be seen. The valence band, near −15 eV, shows the hybridization of O 2p and V 3d orbitals. The band-gap of 3 eV energy width, falls into the valence band and splits the regions where the O 2p states (below the gap) and V 3d states (above the gap) dominate. The Fermi level crosses the upper valence sub-band revealing the metal character of VO_2.

5. Sb_2O_4

It has been reported that equimolar reaction of V(V) and Sb(III) oxides in N_2 at 1023 K forms the rutile phases $VSbO_4$ and Sb_2O_4 [19].

The total density of states calculations for Sb_2O_4 shows a band at −34 eV corresponding to the hybridization of O 2s with Sb 5s (bottom) and Sb 5p (top) orbitals. In the (−20, −14 eV) region mainly O 2p contributions appear, although there is a small contribution of Sb 5s (near −19 eV) and Sb 5p (around −15 eV) orbitals.

6. $VSbO_4$

Fig. 3 presents the trirutile tetragonal super cell used to model the tridimentional (3D) crystal structure of vanadium antimonate. This superstructure contains the most probable metal–oxygen combinations reported in Ref. [3].

The lattice parameters were those reported from experimental measurements [6]: $a = b = 4.636$ Å and $\acute{c} = 3c$ ($c = 3.048$ Å).

Fig. 4 shows the band structure and density of states for this hypothetical structure. The band at −34 eV is formed basically by O 2s bonding states, although there are some contributions of Sb 5s (at the bottom of the band: −35 eV) and Sb 5p (at the top of the band: −33 eV) orbitals. In this energy region, no subtle V 3d hybridization can be detected. In the (−20, −17 eV) energy range a small band originated basically by Sb 5s orbitals appears; while between −17 and −14 eV there are contributions coming from O 2p states (oxygen–metal bonding).

The peaks at the Fermi level could be related to the presence of vanadium in the mixed V–Sb oxide ($E_F = -10{,}228$ eV). This peak is formed with V 3d (t_{2g}) orbital contributions and some V 3d (e_g) states.

Around −10.23 eV we found contributions from metal V 3d (xy) and V 3d (z^2) states, which are antibonding with the

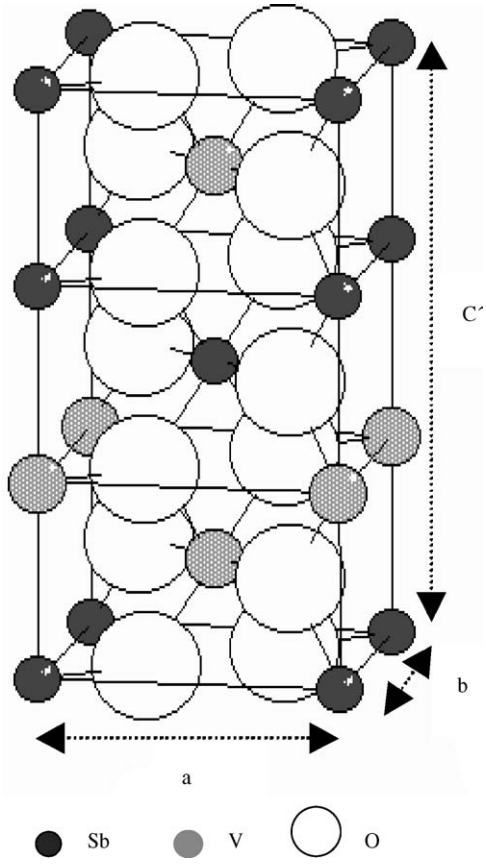

Fig. 3. Superstructure of $VSbO_4$. Lattice parameters: $a = b$, $c' = 3c$.

oxygen atoms similar to that reported in Ref. [20]. Thus, the small band above −10.23 eV could have similar origin.

The COOP curves (Fig. 5) show metal–oxygen bonding interactions (positive region) at −35 and −16 eV, and metal–oxygen antibonding interactions (negative region) around the Fermi level. Moreover, we do not observe metal–metal or oxygen–oxygen interactions in the V–Sb oxide rutile phase.

The (Sb–O) COOP curve in Fig. 5a shows that the band at −35 eV corresponds to O 2s—Sb 5s and Sb 5p bonding orbitals. Around −16 eV we have found bonding between O

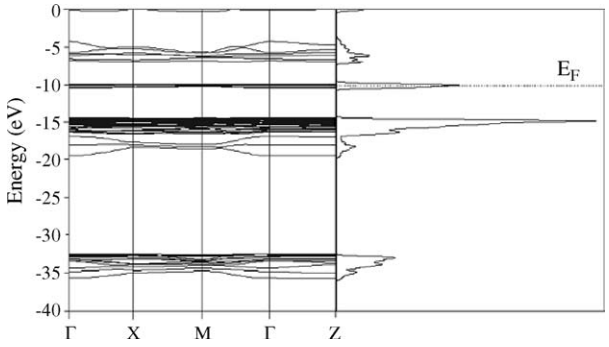

Fig. 4. Band structure along selected symmetry points (left) and total density of states (right) for the crystal 3D structure of $VSbO_4$. The doted line indicates the Fermi level (E_F).

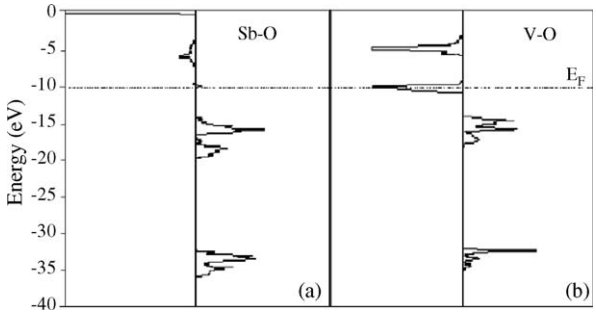

Fig. 5. COOP (metal–oxygen) in the crystal 3D $VSbO_4$ structure. (a) COOP (Sb–O), (b) COOP (V–O). The doted line indicates the Fermi level (E_F).

2p orbitals and Sb 5s and Sb 5p. Above the Fermi level the Sb–O 2p interactions are antibonding.

The (V–O) COOP curve in Fig. 5b shows that the band at −35 eV exhibits bonding contributions coming from O 2s to V 4s orbitals. Around −16 eV we found bonding contributions of O 2p with V 3d states and something of V 4p orbitals. Moreover, a negative peak can be seen at −10 eV coming from the V 3d–O 2p antibonding interaction. Above the Fermi level (near to −5 eV) we detected antibonding V 3d–O 2s and O 2p interactions.

The electronic structure of $VSbO_4$ is similar to the one reported from LCAO-APW calculations for several transition metal dioxides with rutile structure (RuO_2, OsO_2 and IrO_2) [21].

7. Ti-doped V–Sb oxide

$VSbO_4$ presents two redox couples Sb^{3+}/Sb^{5+} and V^{3+}/V^{4+}, whose ratios are modified by the incorporation of foreign ions in the rutile structure. This affects the activity and selectivity of catalytic reactions [22]. Particularly, partial substitution of Sb^{5+} by Ti^{4+} causes V^{3+}oxidation to V^{4+} [6].

Thus, we have studied the effect of antimony partial substitution by titanium in the vanadium antimonate rutile phase. The three-dimensional (3D) tetragonal rutile-type superstructure employed in the calculations represents the $VSb_{0.83}Ti_{0.17}O_4$ catalyst, an ideal solid resulting from a substitution of 17% of the antimony cations by titanium cations.

The total density of states of $VSb_{0.83}Ti_{0.17}O_4$ oxide (V–Sb–Ti) exhibits the major characteristics of that of $VSbO_4$ (V–Sb) with a small peak at −8.5 eV corresponding to empty Ti 4s states.

In Table 2, we report the average charges of Sb, V and O ions in the 3D rutile-type structure of V–Sb and V–Sb–Ti oxides. It can be seen that Ti doping favors vanadium cations oxidation while antimony cations become slightly reduced.

Temperature programmed reduction profiles for V–Sb and V–Sb–Ti (antimony partially substituted by titanium) oxides are plotted in Fig. 6. The profiles for V–Sb and

Table 2
Average charges for Sb, V and O ions in the rutile V–Sb and V–Sb–Ti phases

	Sb	V	O
VSbO4	2.832	1.371	−0.965
$VSb_{0.83}Ti_{0.17}O_4$	2.828	1.494	−1.049

V–Sb–Ti samples show two centers of reduction. Looking at the TPR curves of these samples and those of the pure oxides and the $VSbO_4 + V_2O_5$ mechanical mixture, it leads to the fact that the TPR signals of V–Sb and V–Sb–Ti oxides represent the behavior of the redox couples in the antimonate rutile phase.

Comparing the profile of V–Sb–Ti sample (see Fig. 6c) with that of the V–Sb (see Fig. 6e), it can be seen that the first peak appears at a lower temperature, while the second peak slightly moves to a higher temperature. This fact indicates that antimony partial substitution by titanium increases the oxidation state of vanadium, which matches the results of the Theoretical section.

In addition, the electron population analyses of V–Sb and V–Sb–Ti oxides (see Table 3) show that vanadium oxidizes mainly through a depopulation of V 3d (e_g) orbitals. In the unit cell, the most oxidized V cation shows a depopulation of the V 3d (z^2) orbital close to 41% while for the V 3d (xy) is about 21%.

In Fig. 7, we show the projected V 3d (z^2) density of states in V–Sb–Ti oxide. It can be seen that an important electron density contribution appears at the Fermi level. At this

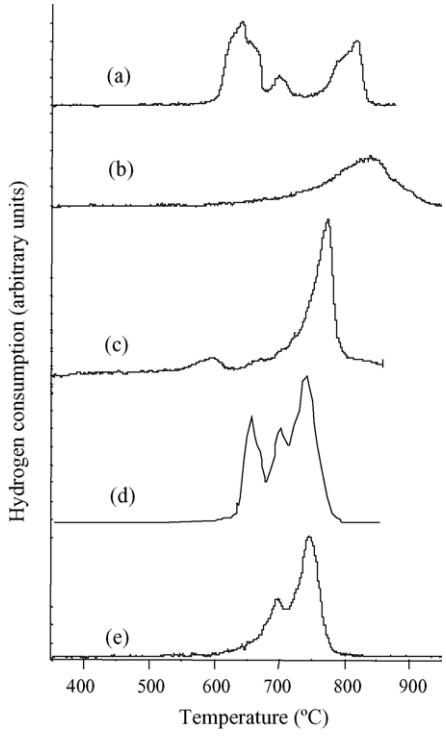

Fig. 6. TPR profiles for V and Sb simple and mixed oxides. (a) V_2O_5, (b) Sb_2O_4, (c) $VSb_{0.8}Ti_{0.2}O_4$, (d) $VSbO_4 + V_2O_5$ (mechanical mixture) and (e) $VSbO_4$.

Table 3
Electron density of the most oxidize V-cation in rutile V–Sb–Ti phase

	4s	4p			3d				
		x	y	z	x^2-y^2	z^2	xy	xz	yz
V–Sb	0.21	0.11	0.16	0.05	1.25	0.39	0.39	0.38	0.39
V–Sb–Ti	0.21	0.11	0.16	0.04	1.15	0.23	0.31	0.37	0.38

energy region, the V–O interactions are of antibonding character. At the same time, we have detected a reinforcement in the involved metal–oxygen bonds.

Our previous calculations of toluene oxidation reactions on $VSbO_4$(1 1 0) indicate that hydrocarbon parallel interaction on Sb–V sites results in the weakening of one of the C–H bonds of the methyl fragment [5]. This leads to an H-abstraction that involves the participation of an Sb-cation. Moreover, the theoretical results reveal that after toluene H-abstraction the non-bonding phenyl–V interaction facilitates benzyl-type species desorption. This interaction involves the V 3d states located at the Fermi level of the solid.

When antimony is partially substituted by titanium in V–Sb oxides the presence of more oxidized V-cations, with the concomitant reinforcement of their V–O bonds, suggests that toluene parallel adsorption on Sb–V sites could be favored. That is, phenyl–V non-bonding interaction increases favoring the electron transference from the methyl group to the solid. Thus, the C_{methyl}–H bond weakens and the benzyl-type species desorption enhances.

In a previous experimental work, we have found that, in toluene oxidation on vanadium antimonate, a direct relationship between the hydrocarbon conversion and the V^{4+}/Sb^{5+} ratio is present [23]. This fact leads to the conclusion that catalyst oxidation is the rate limiting step and that both cations vanadium and antimony participate in the mechanism of partial oxidation.

It is known that mixed effective catalyst in partial oxidation reactions must have a redox couple with a reduction potential greater than that of the element inserting oxygen into the hydrocarbon molecule. In this way faster

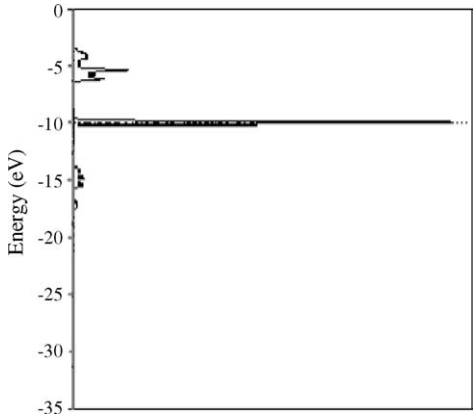

Fig. 7. Projected density of states of V 3d (z^2) orbitals in the crystal 3D structure of $VSbO_4$. The doted line indicates the Fermi level (E_F).

active sites reoxidation is promoted and the catalyst remains active. In catalyst based on antimonates, it has been reported that V^{4+} cations reoxidize the metal-cations which insert oxygen into the hydrocarbon fragment to give oxygenate products [4]. The V^{4+} cations while incorporating gaseous oxygen as lattice oxygen hold the Sb sites in an oxidation state high enough to insert oxygen into the hydrocarbon fragment to give partial oxidation products (benzaldehyde). Carbon oxides formation involves the participation of the V–O–V species as mentioned in Section 1.

Thus, our results show that Sb partial substitution by Ti in V–Sb oxides enhances both the activity and selectivity of these catalysts in toluene oxidation reactions.

8. Conclusions

The electronic analysis of the $VSbO_4$ structure shows similarities with that of other simple transition metal oxides with rutile structure. Moreover, the presence of vanadium in the solid originates the peak at the Fermi level of the total density of states curve. This is in agreement with the metal character that vanadium gives to VO_2 in the rutile phase of high temperature.

On the other hand, Ti doping of the V–Sb oxides by partial substitution of Sb would increase the number of vanadium cations in higher oxidation state. Thus, the concomitant depopulation of their antibonding V 3d states located at the Fermi level should favor toluene aromatic ring antibonding interactions on these V-cation sites. This fact enhances the rate of the H-abstraction and benzyl-type species desorption stage. In addition, a faster reoxidation of the antimony surface sites reduced by oxygen insertion into the hydrocarbon fragment to give benzaldehyde would be expected by the modification of the catalyst V^{3+}/V^{4+} ratio.

Then, antimony partial substitution by titanium in vanadium antimonate provides vanadium cations in higher oxidation states which can easily reoxidize the Sb surface active sites improving the catalyst activity and selectivity.

Acknowledgements

Our work was supported by Universidad de Buenos Aires, Fundación Antorchas, ANPCYT (PICT 12-09857), CONICET PEI 98 and Departamento de Física, Universidad Nacional del Sur.

References

[1] R.K. Grasselli, Catal. Today 49 (1999) 141.
[2] T. Birchall, A.W. Sleight, Inorg. Chem. 15 (4) (1976) 868.
[3] S. Hansen, K. Ståhl, R. Nilsson, A. Andersson, J. Solid State Chem. 102 (1993) 340.
[4] R.K. Grasselli, in: H. Knozinger, J. Weitkamp (Eds.), Handbook of Heterogeneous Catalysis: Amoxidation, vol. 5, Wiley, New York, 1997, p. 2302.
[5] B. Irigoyen, A. Juan, S. Larrondo, N. Amadeo, J. Catal. 201 (2001) 169.
[6] F.J. Berry, L.E. Smart, S. Duhalde, Polyhedron 15 (24) (1996) 651.
[7] R. Hoffmann, W.N. Lipscomb, J. Chem. Phys. 36 (1962) 2179.
[8] R. Hoffmann, J. Chem. Phys. 39 (1963) 1397.
[9] R. Hoffmann (Ed.), Solids and Surfaces: A Chemist's View of Bonding in Extended Structures, Wiley–VCH, New York, 1988.
[10] G. Landrum, YAeHMOP, Cornell University, 1997, Yaehmop is available at http://www.overlap.chem.cornell.edu:8080/yaehmop.html.
[11] B. Irigoyen, A. Juan, S. Larrondo, N. Amadeo, Surf. Sci. 523 (2003) 252.
[12] P. Kubácek, R. Hoffmann, Z. Havlas, Organometallics 1 (1982) 180.
[13] T. Hughbanks, R. Hoffmann, M.H. Whangbo, K.R. Stewart, O. Eisenstein, E. Canadell, J. Am. Chem. Soc. 104 (1982) 3876.
[14] J.H. Ammeter, H.B. Bürgi, J.C. Thibeaut, R. Hoffmann, J. Am. Chem. Soc. 100 (1978) 3686.
[15] R. Ramirez, M.C. Böhm, Int. J. Quantum Chem. 30 (1986) 391.
[16] R. Ramirez, M.C. Böhm, Int. J. Quantum Chem. 34 (1988) 571.
[17] L.A. Grunes, R.D. Leapman, C.N. Wilker, R. Hoffmann, Phys. Rev. B 25 (1982) 7157.
[18] W.H. Strehlow, E.L. Cook, J. Phys. Chem. Ref. Data 2 (1973) 163.
[19] F.J. Berry, M.E. Brett, W.R. Patterson, J. Chem. Soc. Dalton Trans. 9 (1983).
[20] J.K. Burdett, T. Hughbanks, Inorg. Chem. 24 (1985) 1741.
[21] L.F. Mattheiss, Phys. Rev. B 13 (1976) 2433.
[22] G. Centi, E. Foresti, F. Guarneri, in: V., Cortés Corberán, S., Vic Bellón (Eds.), New Developments in Selective Oxidation II, vol. 82, 1994, p. 293.
[23] S. Larrondo, B. Irigoyen, G. Baronetti, N. Amadeo, Appl. Catal. A 250 (2003) 279.